OncoTargets and Therapy

Dovepress
Taylor & Francis Group

Open Access Full Text Article

ORIGINAL RESEARCH

CD93: A Promising NETs-Related Biomarker for Diagnosis and Therapy in Actinic Keratosis

Guolin Ke[1–5], Tao Yuan[2], Chen Wu[2], Min Gao[1,3–5]

[1]Department of Dermatology, The First Affiliated Hospital, Anhui Medical University, Hefei, Anhui, 230032, People's Republic of China; [2]Department of Dermatology and Venereology, The First Affiliated Hospital, Wannan Medical College, Wuhu, Anhui, 241001, People's Republic of China; [3]Institute of Dermatology, Anhui Medical University, Hefei, Anhui, 230032, People's Republic of China; [4]Key Laboratory of Dermatology (Anhui Medical University), Ministry of Education, Hefei, Anhui, 230032, People's Republic of China; [5]Collaborative Innovation Center of Complex and Severe Skin Disease, Anhui Medical University, Hefei, Anhui, 230032, People's Republic of China

Correspondence: Min Gao, Department of Dermatology, The First Affiliated Hospital, Anhui Medical University, Hefei, Anhui, 230032, People's Republic of China, Email ahhngm@163.com

Background: Actinic keratosis (AK), a UV-induced precancerous skin condition potentially progressing to cutaneous squamous cell carcinoma (cSCC) with undefined mechanisms, was analyzed for neutrophil extracellular traps (NETs)-related biomarkers to identify key clinical targets.

Methods: Transcriptomic profiles of AK retrieved from the GEO database were analyzed using the "limma" package to screen differentially expressed genes (DEGs), which were intersected with a curated NETs-related gene set to extract differentially expressed NETs-related genes (DE-NRGs). Functional enrichment analyses via Gene Ontology (GO) and Kyoto Encyclopedia of Genes and Genomes (KEGG) annotations identified enriched biological processes and pathways. Diagnostic biomarkers were screened using LASSO regression, random forest (RF), and Support Vector Machine Recursive Feature Elimination (SVM-RFE), with performance assessed by receiver operating characteristic (ROC) curves. Clinical validation compared CD93-positive microvessel density (CD93-MVD) levels between 53 AK samples and normal skin controls. Single-sample gene set enrichment analysis (ssGSEA) evaluated immune cell infiltration and neutrophil-related pathway activity, while molecular docking screened potential CD93-targeting drugs.

Results: Nine DE-NRGs were identified by comparing AK samples with controls. GO/KEGG enrichment highlighted neutrophil chemotaxis, migration, and IL-17 signaling pathways. LASSO, RF, and SVM-RFE selected CD93 as a key diagnostic biomarker, showing overexpression in training (GSE207744, AUC=0.863) and validation (GSE32628, AUC=0.956) datasets. Immunohistochemistry confirmed significantly higher CD93-MVD levels between AK and normal skin ($p=5.36\times10^{-11}$), with elevation in elderly patients (p=0.042), multifocal lesions (p=0.028), and with increasing severity (clinical: p=0.040; dermoscopic: p=0.007; pathological: $p=2.3\times10^{-6}$). ssGSEA revealed increased immune cell infiltration and neutrophil pathway activity in AK. Molecular docking identified Gö6976 as a CD93 inhibitor (ΔG=−7.5 kcal/mol).

Conclusion: Our study establishes CD93 as a key NETs-related biomarker in AK, mechanistically linking neutrophil-driven inflammation to angiogenesis. The CD93-Gö6976 interaction provides a translational basis for developing novel targeted therapies against AK.

Keywords: actinic keratosis, AK, neutrophil extracellular traps, NETs, CD93, biomarker, targeted therapy

Introduction

Actinic keratosis (AK), a prevalent ultraviolet radiation-induced precancerous dermatosis, clinically presents as erythematous, skin-toned, or hyperpigmented macules/patches with adherent keratotic scales. These lesions are predominantly localized to long-term photo-damaged cutaneous regions, with a markedly increased incidence in geriatric populations. Characteristic epidermal dysplasia, characterized by disordered proliferation of atypical keratinocytes within the stratum spinosum and manifesting as nuclear pleomorphism, loss of cellular polarity, and abnormal differentiation patterns, represents the histopathological features of AK.[1] These dysplastic lesions demonstrate malignant transformation potential, with epidemiological studies estimating that approximately 65% of cutaneous squamous cell carcinoma (cSCC)

Received: 24 May 2025
Accepted: 12 August 2025
Published: 27 August 2025

cases originate from AK precursor lesions.[2] The prevalence of AK among Caucasian individuals over 40 years old ranges from 11% to 60%.[3] Population aging has driven a steady annual increase in AK incidence rates.[4] Despite the high prevalence of AK and its recognized potential for malignant transformation, the molecular mechanisms underlying AK pathogenesis remain poorly characterized at the transcriptional and cellular levels.

Neutrophils are polymorphonuclear cells and are considered principal effector cells in the innate immune response. Their classical antimicrobial mechanisms include phagocytosis and degranulation.[5] Activated neutrophils secrete neutrophil extracellular traps (NETs)—web-structured assemblies blending DNA, histones, and antimicrobial peptides.[6] As a distinct programmed cell death modality (NETosis) differing from classical apoptosis and oncotic necrosis, NETs possess a unique mesh-like structure that facilitates microbial entrapment and neutralization, thereby conferring innate immune protection through pathogen immobilization and clearance.[7] However, excessive release of NETs can have detrimental effects on the host.[8] Recent research highlights the NETs' pivotal involvement in the pathogenesis of certain metabolic disorders such as Type 2 diabetes,[9] autoimmune conditions including psoriasis[10] and systemic lupus erythematosus (SLE),[11] autoinflammatory diseases such as Gout,[12] and certain tumors such as malignant melanoma.[13] Currently, no definitive evidence has established NETs as directly associated with AK in pathogenic mechanisms. However, preclinical evidence from cSCC—a malignant counterpart of AK—highlights notable NETs involvement, with 79.2% of cSCC specimens demonstrating NETs expression. This expression correlates significantly with tumor ulceration and abscess-like structures, paralleling the dense neutrophil infiltration observed in 75% of cSCC cases, where infiltration density positively correlates with tumor cross-sectional area. Mechanistically, while global CD8+ T cell infiltration is unaltered in NETs-positive cSCC, these cytotoxic T cells are notably absent in neutrophil swarming zones, suggesting NETs-mediated modulation of the local tumor microenvironment.[14] Given AK's status as a premalignant lesion of cSCC and the known release of NETs under inflammatory/injury conditions, we hypothesize a role for NETs in AK pathogenesis. AK is characterized by dysregulated keratinocyte hyperproliferation, aberrant keratinization, and chronic UV-induced low-grade inflammation—microenvironmental conditions that may promote NETosis. Considering NETs' established role in cutaneous inflammatory signaling and immunomodulation, we postulate their contribution to AK progression. Herein, we conducted comprehensive bioinformatics analyses to identify differentially expressed NETs-related genes (DE-NRGs) and investigate their potential roles in AK pathogenesis. Through combined immune infiltration profiling and molecular docking validation, we established CD93 as a key biomarker with dual diagnostic and therapeutic significance. Immunohistochemical analysis further demonstrated significant correlations between CD93-MVD and critical clinical parameters: advanced age (p=0.042), multifocal lesions (p=0.028), as well as disease severity assessed by clinical (p=0.040), dermoscopic (p=0.007), and histopathological grading (p=2.3×10^{-6}). These findings provide mechanistic insights for developing AK-specific diagnostic strategies and targeted therapies. The experimental workflow is systematically presented in Figure 1.

Methods

Data Download

From the GEO database, RNA-seq datasets for this study were retrieved, encompassing 116 samples across four distinct datasets. GSE207744 included 45 samples (21 AK cases and 24controls), GSE142108 contained 30 (15 AK cases and 15 controls), GSE32628 held 27 (14 AK cases and 13 controls), and GSE90643 comprised 14 (7 AK cases and 7 controls). As the training cohort, GSE207744 was designated, while GSE142108, GSE32628, and GSE90643 served as validation cohorts. Dataset specifics are summarized in Table 1. Notably, the 69 NETs -related biomarkers incorporated in this analysis were carefully curated from prior research,[15] with detailed data listed in Supplementary Table S1.

Screening of Differential Expressed NETs-Related Genes

Initially, differential expression analysis was implemented on GSE207744 via the "Deseq2" package (version 1.38.2).[20] We set thresholds as p-value <0.05 and |logFC|>1, 9 DE-NRGs were identified through intersection analysis between DEGs from AK versus control samples and the 69 pre-established NRGs.

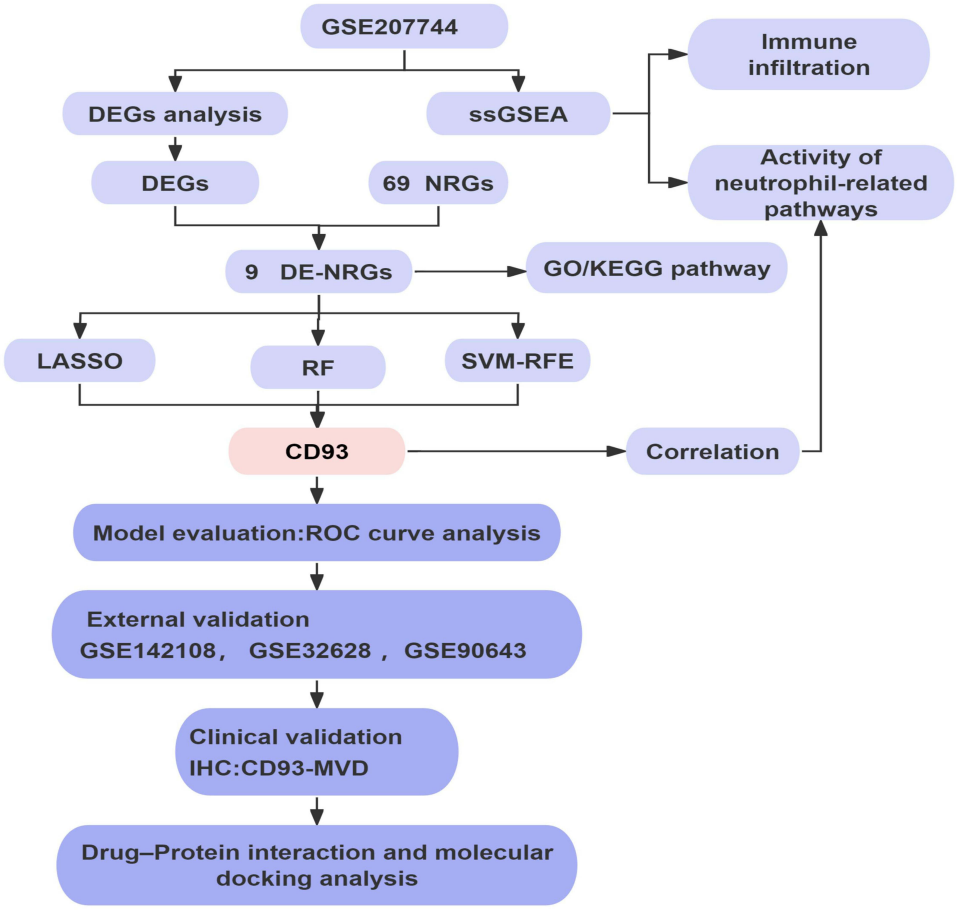

Figure 1 The flowchart of the study.

Functional Enrichment Profiling of Differential Expressed NETs-Related Genes

To dissect functional implications, GO analysis pinpointed critical biological processes (BP), cellular components (CC), and molecular function (MF) annotations that contextualize DE-NRGs' roles.[21] KEGG, an integrated platform for mapping metabolic networks, was employed to identify enriched pathways among DE-NRGs.[22] Leveraging the robust

Table 1 GEO Data Set Information List

Dataset	GSE207744	GSE142108	GSE32628	GSE90643
Usage	Training dataset	Validation dataset	Validation dataset	Validation dataset
Platform	GPL21185	GPL23159	GPL6102	GPL570
Species	Homo sapiens	Homo sapiens	Homo sapiens	Homo sapiens
Samples in the disease group	21	15	14	7
Samples in the control group	24	15	13	7
Reference	Dubois-Pot-Schneider H, Khairallah G, Brzenczek C, Plénat F, Marchal F, Amouroux M. Transcriptomic Study on Human Skin Samples: Identification of Two Subclasses of Actinic Keratoses. Int J Mol Sci. 2023;24(6):5937.[16]	Segura S, Gadea A, Nonell L et al. Identification of differentially expressed genes in actinic keratosis samples treated with ingenol mebutate gel. *PLoS One*. 2020;15(5): e0232146.[17]	Hameetman L, Commandeur S, Bavinck JN, et al. Molecular profiling of cutaneous squamous cell carcinomas and actinic keratoses from organ transplant recipients. BMC Cancer. 2013;13:58.[18]	Joly F, Deret S, Gamboa B, et al. Photodynamic therapy corrects abnormal cancer-associated gene expression observed in actinic keratosis lesions and induces a remodeling effect in photodamaged skin. J Dermatol Sci. Published online May 17, 2018.[19]

https://doi.org/10.2147/OTT.S539790

R package "clusterProfiler" (version 4.10.0), GO/KEGG enrichment profiling ($p < 0.05$) of the DE-NRGs was performed.[23] Visually compelling bar charts were subsequently generated via the "ggplot2" package (version 3.5.1).

Identification of NETs-Related Diagnostic Biomarkers

For identifying NETs-related biomarkers, three advanced analytical methods were utilized: LASSO regression, random forest (RF), and Support Vector Machine Recursive Feature Elimination (SVM-RFE). With the aim of enhancing prediction precision through variable selection, LASSO—a frequently applied regression strategy—is implemented using the "glmnet" R package (version 4.1). To diminish potential bias, the optimal λ value is selected, and genes with partial collinearity are removed.[24] Leveraging the "randomForest" R package (version 4.7), the RF algorithm—a supervised classification method that aggregates multiple decision trees—was employed.[25] Error rates for tree counts ranging from 1 to 500 were evaluated. Following the selection of the optimal tree number based on the lowest error rate, the RF algorithm assessed variable importance via the MeanDecreaseGini metric, with genes showing values surpassing 3 designated as candidate biomarkers for follow-up analysis. We assessed the SVM-RFE model—a novel machine learning technique capable of recursively ranking features to mitigate overfitting—using average misclassification rates from 10-fold cross-validation via the "e1071" R package.[26] Through the intersection of key genes identified by LASSO, RF, and SVM-RFE, NETs-related diagnostic biomarkers were obtained.

Receiver Operating Characteristic Curve (ROC) Analysis for NETs-Related Diagnostic Biomarkers

To validate the clinical utility of NETs-related diagnostic biomarkers in AK, we employed the "pROC" R package to compute ROC curves, thereby assessing their diagnostic performance.[27] Regarding the generation of ROC curves, the "pROC" R package is esteemed for two principal strengths. Firstly, its specialized design enables exact curve computation and the provision of detailed statistical indicators. Secondly, its efficient and user-friendly interface guarantees dependable results with minimal operational exertion.

Immunohistochemistry Staining

From December 2022 through October 2024, 53 formalin-fixed, paraffin-embedded tissue specimens of AK skin lesions and 20 specimens of normal skin tissue circumjacent to the nevus were collected at the First Affiliated Hospital of Wannan Medical College. This study received approval from the Ethics Committee of the First Affiliated Hospital of Wannan Medical College (No. 2024–178). Informed consent was obtained and signed by all human participants. Written consent for the publication of these details has been secured from each of them. Primary antibodies applied for the assays were: Polyclonal rabbit anti-CD93 (cat. no. 18283-1-AP; 1:600 dilution; Wuhan, China). The IHC assay was conducted as previously reported.[28] The MVD count, which is marked by CD93, is conducted in line with the method put forward by Weidner et al.[29] Specifically, under low-power (×40) magnification, the hotspot area - defined as the lesion area exhibiting the highest microvessel density - is first identified. Then, within this area, the MVD count is completed by counting the number of microvessels under high-power magnification (×200). During the counting process, the morphological characteristics of microvessels are used as the basis for judgment. Any vascular structure that is stained brown and has a complete outline is considered a microvessel for counting.

Single Sample Gene Set Enrichment Analysis (ssGSEA)

Through ssGSEA, we evaluated the enrichment degree of pre-established gene sets in each sample. This empowers researchers to measure the activity of biological pathways or signatures within a solitary specimen. Widely embraced in bioinformatics, especially in immunology and cancer research, this methodology enables single-sample pathway profiling.[30] Analyzing the modifications in biological pathways related to neutrophils within AK samples and control samples, as well as the variations in 28 immune cell types, we have employed this technique.

Analysis of Drug - Protein Binding Interaction and Molecular Docking for NETs - Associated Diagnostic Biomarkers

Search Tool for Interacting Chemicals (STITCH) is a comprehensive database that compiles data on chemical-protein interactions, enabling the identification and analysis of networks between small molecules-like drugs, metabolites, and toxins—and proteins.[31] Data on potential drug targets associated with these genes were retrieved from the STITCH database (http://stitch.embl.de/) by inputting the identified NETs - related diagnostic biomarkers. From the AlphaFold Protein Structure Database (https://alphafold.ebi.ac.uk/) and the PubChem Database (https://pubchem.ncbi.nlm.nih.gov/), the 3D configurations of the target proteins and their corresponding drugs were acquired.[32,33] Docking simulations and visualization analyses were performed using PyMOL(version 2.4.0)and AutoDock Vina (version 1.2.0).[34]

Statistical Analysis

We performed all statistical analyses via R software (version 4.3.2). We assessed the normality of continuous variables using the Lilliefors test. For non-normally distributed data, we reported the median with interquartile range (IQR). Multi-group comparisons were initially analyzed using the Kruskal–Wallis rank- sum test, followed by post hoc pairwise comparisons using the Wilcoxon rank-sum test with Bonferroni correction to adjust for multiple testing. The chi-square test was applied to analyze categorical variables when the assumptions were met; otherwise, Fisher's exact test was used. Statistical significance was defined as a two - tailed p - value of < 0.05.

Results

Screening of Differential Expressed NETs-Related Genes

A comprehensive analysis using the GSE207744 dataset was conducted to explore the role of NRGs in AK pathogenesis. GSE207744 includes 72 tissue samples in total, comprising 23 squamous cell carcinomas (SCC), 21 AK lesions, and 28 healthy control specimens. The healthy controls include 24 non-lesional sites and 4 perilesional lesions. From this dataset, we specifically selected 21 AK samples and 24 non-lesional lesion samples (control group) for our rigorous analysis. Differential analysis across the AK and control groups uncovered 275 DEGs, comprising 192 upregulated and 83 downregulated genes (Supplementary Table S2). The dispersion of these DEGs was effectively visualized via a volcano plot (Figure 2A). Gene expression across different groups was also visualized using a heat map (Figure 2B). The DEG list was intersected with 69 established NRGs, yielding a subset of 9 DE-NRGs (Figure 2C; Supplementary Table S3). Through GO enrichment analysis of the DE-NRGs, we found their involvement in neutrophil chemotaxis, neutrophil migration and neutrophil mediated immunity. Additionally, the activation of signaling pathways, including the IL-17 and PI3K−Akt pathways, was identified via KEGG pathway analysis (Figure 2D, E and Supplementary Tables S4 and S5).

Identification of NETs-Related Diagnostic Biomarkers

Three machine learning algorithms were employed in the training set GSE207744 to identify featured genes from candidate key genes in AK patients. During LASSO algorithm-based screening, 5 of 9 NETs-related genes with non-zero coefficients were derived (Figure 3A and B). RF modeling was subsequently employed to evaluate feature importance, with genes exhibiting a MeanDecreaseGini score >3 being extracted (Figure 3C and D). Through SVM-RFE feature selection, three genes were identified as top candidates for AK (Figure 3E and F). Ultimately, cross-analysis of candidate genes from LASSO, RF, and SVM-RFE models identified CD93 as a NETs-related biomarker for subsequent validation in AK (Figure 3G and Supplementary Table S6).

CD93 Diagnostic Performance for AK in Training and Validation Datasets

CD93 exhibited marked upregulation in the AK group versus the control group in both training set GSE207744 and validation set GSE32628 ($p < 0.05$) (Figure 4A and C). In validation sets GSE142108 and GSE90643, CD93 expression trended higher in the AK group relative to controls, yet this difference failed to achieve statistical significance ($p > 0.05$) (Figure 4B and D). ROC curve analysis was performed to evaluate the diagnostic utility of CD93 in AK. In the training

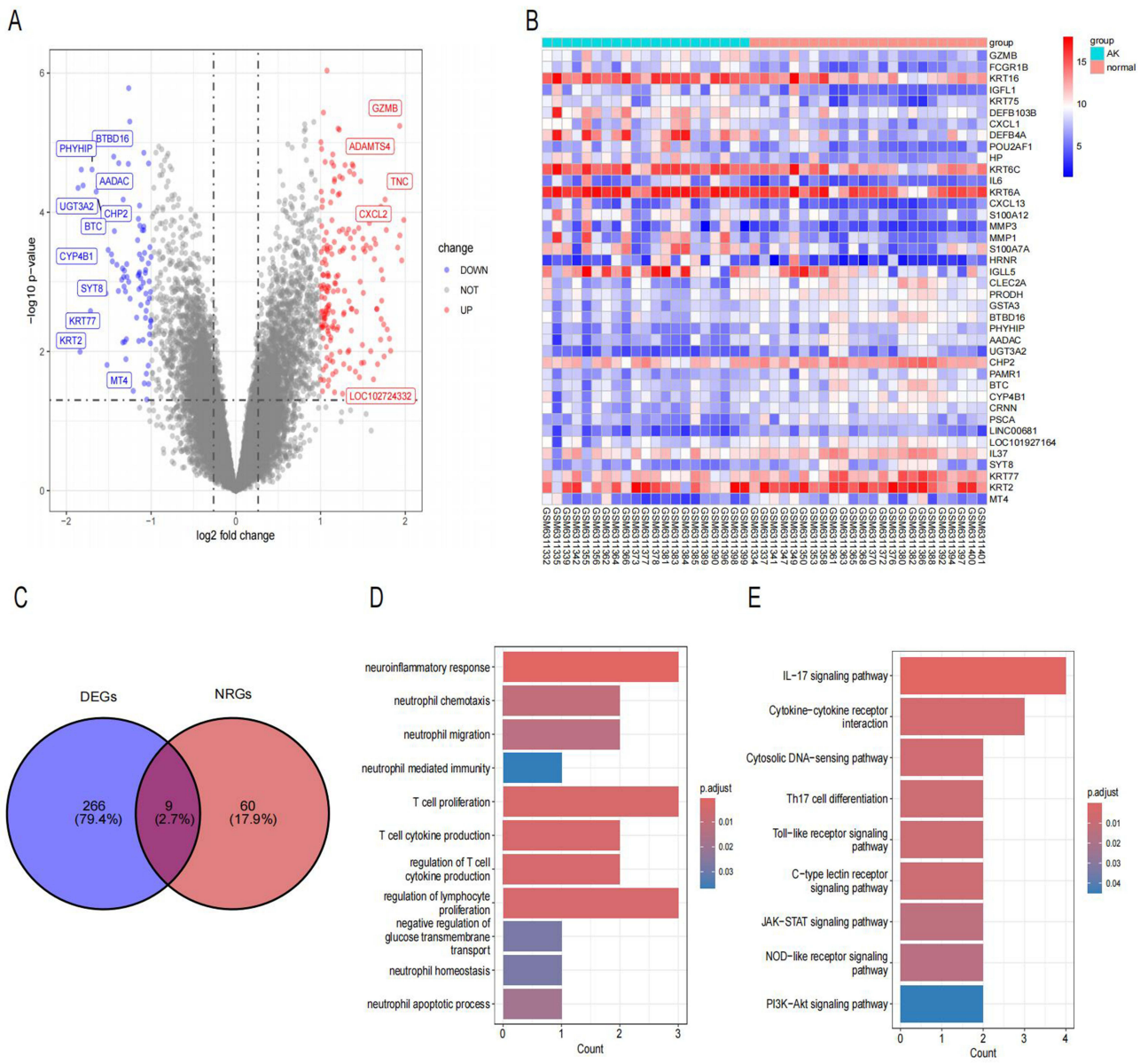

Figure 2 Identification of differentially expressed NETs-related genes. (**A**) Volcano plot of DEGs in GSE207744. (**B**) Heatmap of the top 20 DEGs. (**C**) A Venn diagram of GSE207744 DEGs and NETs-related genes. (**D–E**) GO enrichment and KEGG analysis of NETs-related genes.

dataset (GSE207744), CD93 demonstrated robust diagnostic performance with an AUC of 0.863 (Figure 4E). Across three independent validation datasets (GSE142108, GSE32628, and GSE90643), CD93 achieved AUC values of 0.627, 0.956, and 0.674, respectively (Figure 4F–H), collectively corroborating its diagnostic validity in AK.

Comparison of CD93- MVD Between AK and Normal Skin Tissues

A significant difference in CD93-MVD was detected between AK lesions and normal skin tissue circumjacent to the nevus (Wilcoxon rank-sum test, $p < 0.001$). Quantitative analysis revealed that the CD93-MVD in AK specimens, with a median of 20 (IQR: 17, 25) vessels per high - power field (HPF), was 2.5-fold higher than that in normal control tissues, which had a median of 8 (IQR: 7,9) vessels/HPF (Figure 5A–C).

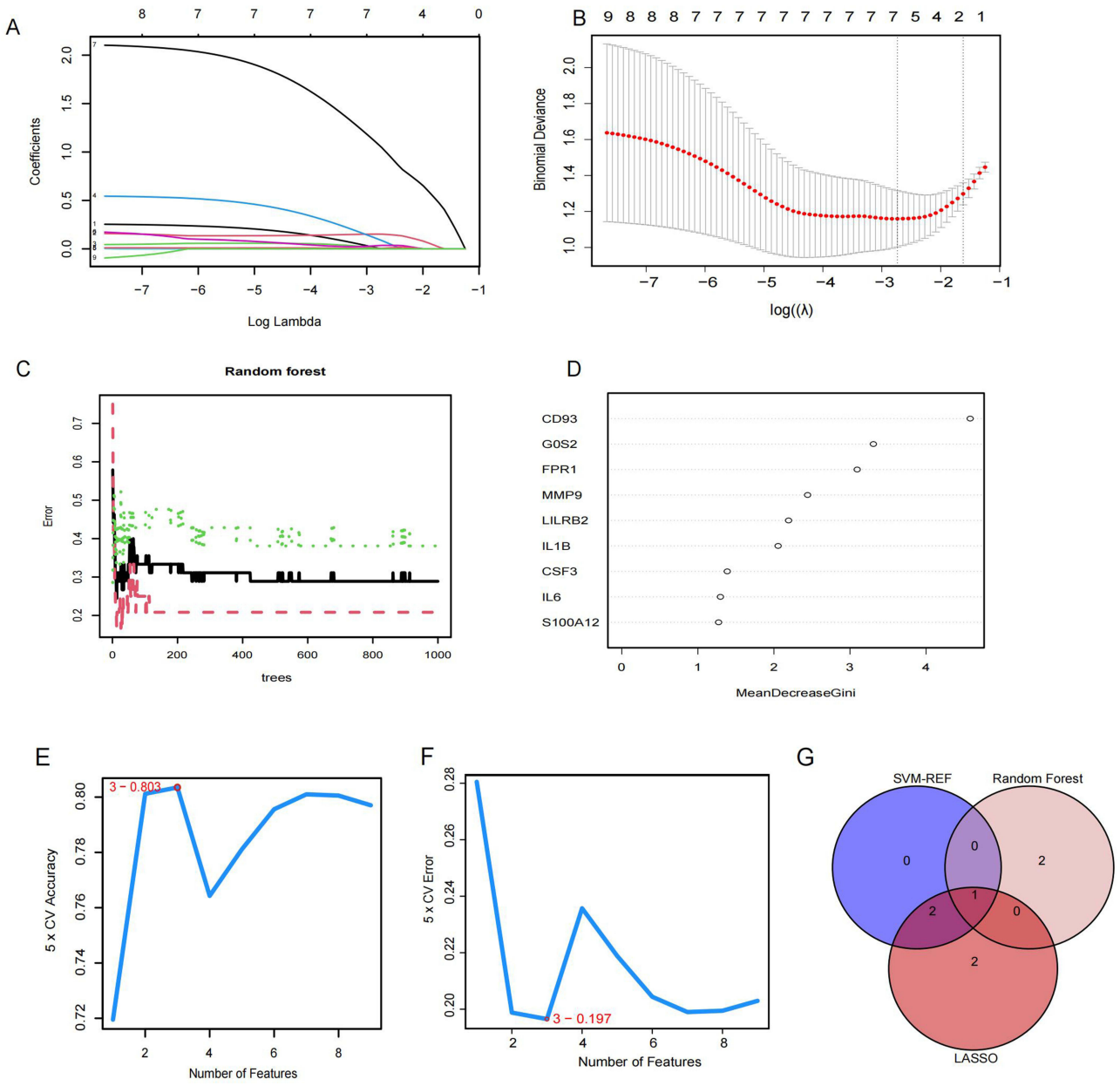

Figure 3 CD93 was identified as a diagnostic biomarker for AK. (**A** and **B**) Regression coefficient path diagram and cross-validation curves in LASSO logistic regression. (**C** and **D**) Feature importance identification via RF. (**E** and **F**) The curve of change in the predicted true and error value of each gene in SVM-RFE algorithm. (**G**) A Venn diagram shows the intersection of diagnostic markers from the three algorithms.

Relationship Between CD93-MVD and Clinical, Dermoscopic, and Pathological Characteristics of AK

This study evaluated 53 histologically confirmed AK cases (14 males, 39 females) with a mean age of 68.11±11.52 years (range: 42–89), stratified into ≤65 years old (n=22) and >65 years old (n=31). The disease course ranged from 3 months to 15 years (≤1 year:13 cases; >1 year:40 cases). Lesion distribution revealed facial predominance (cheeks:32, nose:5, temples:5, forehead:3, scalp:8) with 34 patients presenting multiple lesions versus 19 with solitary lesions. Pathological grading according to Roewert-Huber criteria (n=53) demonstrated grade I (25), II (18), and III (10) differentiation, paralleling dermoscopic (grade I:18, II:25, III:10) and clinical severity classifications (grade I:22, II:19, III:12). Representative clinical, dermoscopic, and pathological features of characteristic cases are illustrated in Figure 6. Further analysis revealed that elderly patients (>65 years old) exhibited elevated CD93-MVD compared to younger counterparts (≤65 years old)(p=0.042),

https://doi.org/10.2147/OTT.S539790

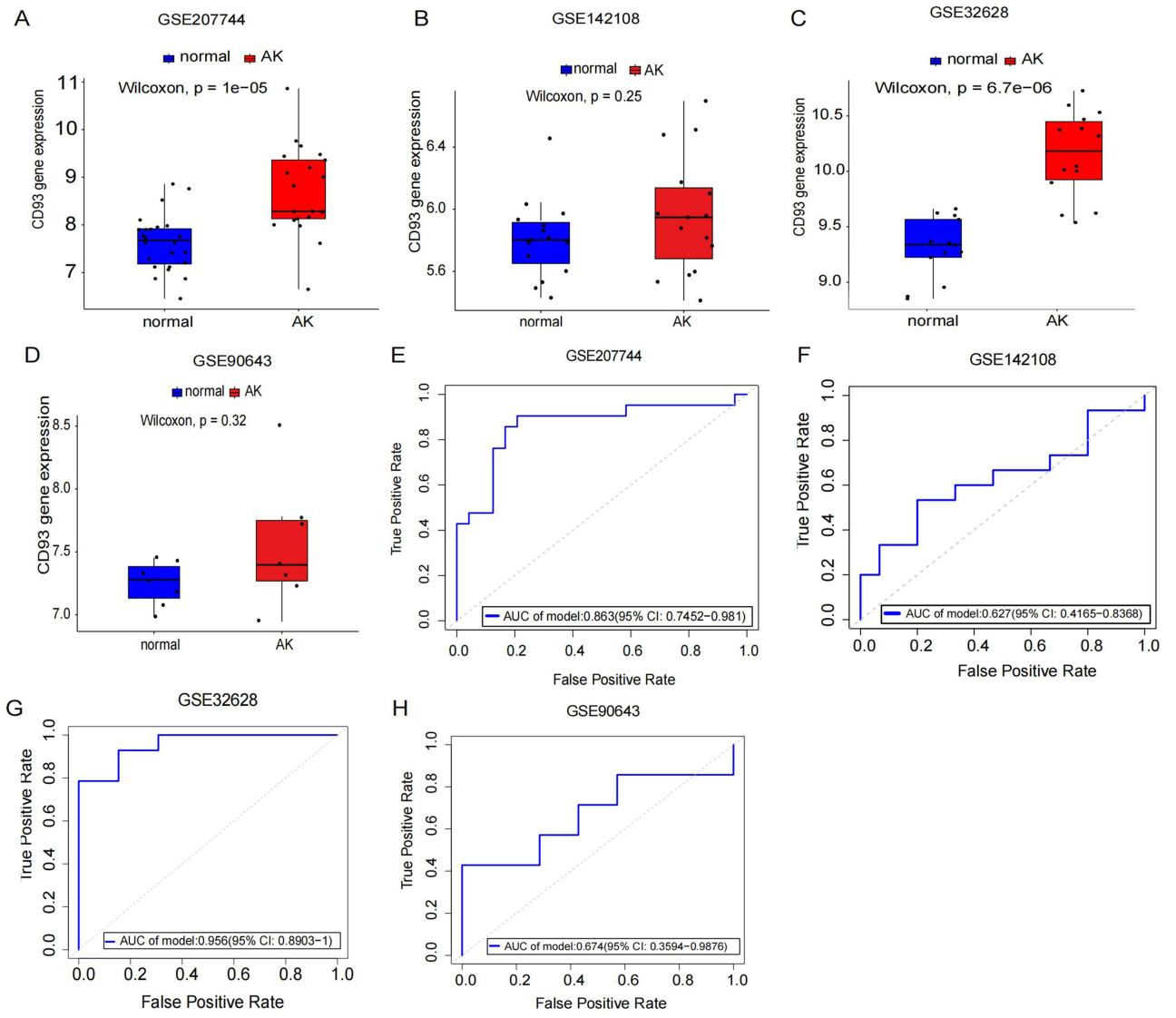

Figure 4 Diagnostic Performance of CD93 for AK in the training set and the validation sets. (**A**–**D**) Box plots showing the expression differences of CD93 between AK and control groups in four datasets. (**A**) GSE207744: Significant upregulation in AK (Wilcoxon, *p* = 1e-05). (**B**) GSE142108: No significant difference (Wilcoxon, p = 0.25). (**C**) GSE32628: Significant upregulation in AK (Wilcoxon, p = 6.7e-06). (**D**) GSE90643: No significant difference (Wilcoxon, p = 0.32). (**E**–**H**) ROC curves depicting the diagnostic performance of CD93 for distinguishing AK from controls in the same datasets. (**E**) GSE207744: AUC=0.863 (95% CI: 0.7452–0.981). (**F**) GSE142108: AUC = 0.627 (95% CI: 0.4165–0.8368). (**G**) GSE32628: AUC=0.956 (95% CI: 0.8903–1). (**H**) GSE90643: AUC = 0.674 (95% CI: 0.3594–0.9876).

while no gender-based (*p*=0.511) or disease course-related differences (*p*=0.634) were observed. Multifocal lesions demonstrated significantly higher vascularization than solitary lesions (*p*=0.028). Progressive CD93-MVD elevation correlated with ascending severity grades across all classification systems: pathological ($p=2.3\text{x}10^{-6}$), dermoscopic (*p*=0.007), and clinical (*p*=0.040) - with statistically significant intergrade differences (Table 2 and Figure 7A–G). These findings position CD93-MVD as a potential biomarker for objectively stratifying AK progression and therapeutic response.

Immune Infiltration and Neutrophil-Related Pathways Analysis

The ssGSEA algorithm was applied to characterize immune cell infiltration profiles between AK and control groups. Significantly higher abundances of activated CD8+ T cells, central memory CD8+ T cells, effector memory CD8+ T cells, central memory CD4+ T cells, effector memory CD4+ T cells, T follicular helper cells, γδ T cells, Th1 cells, Th17 cells, Th2 cells, Tregs, activated B cells, immature B cells, memory B cells, natural killer cells, CD56bright NK cells, CD56dim NK cells, myeloid-derived suppressor cells, NKT cells, activated dendritic cells, plasmacytoid dendritic cells, immature

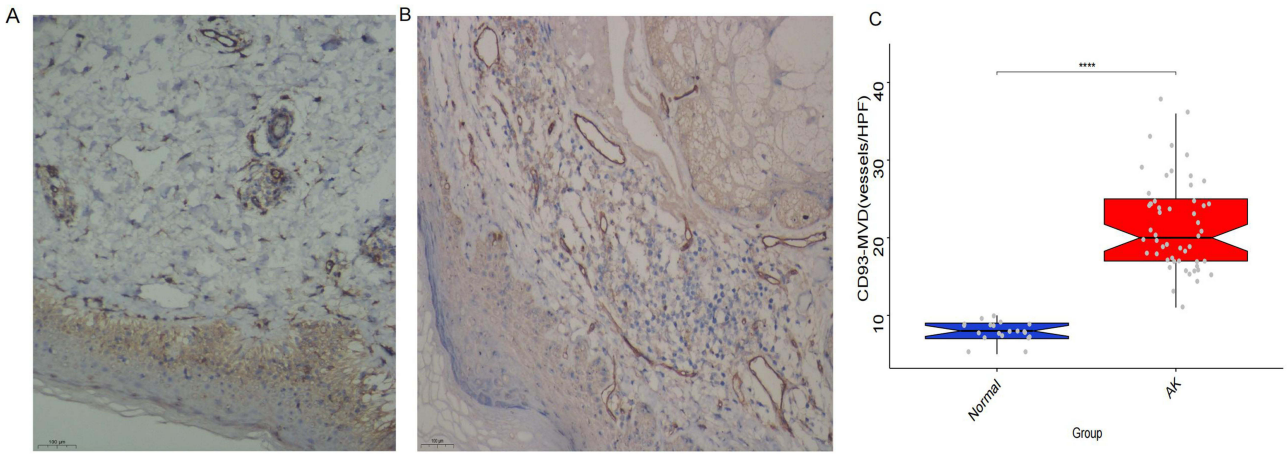

Figure 5 Differences in CD93-MVD levels between normal skin and AK tissues. (**A** and **B**) Immunohistochemical staining of CD93-MVD in normal skin and AK tissues (scale bar: 100μm). (**C**) Box plot showing significantly higher CD93-MVD in the AK group compared to the normal group (****,P < 0.0001).

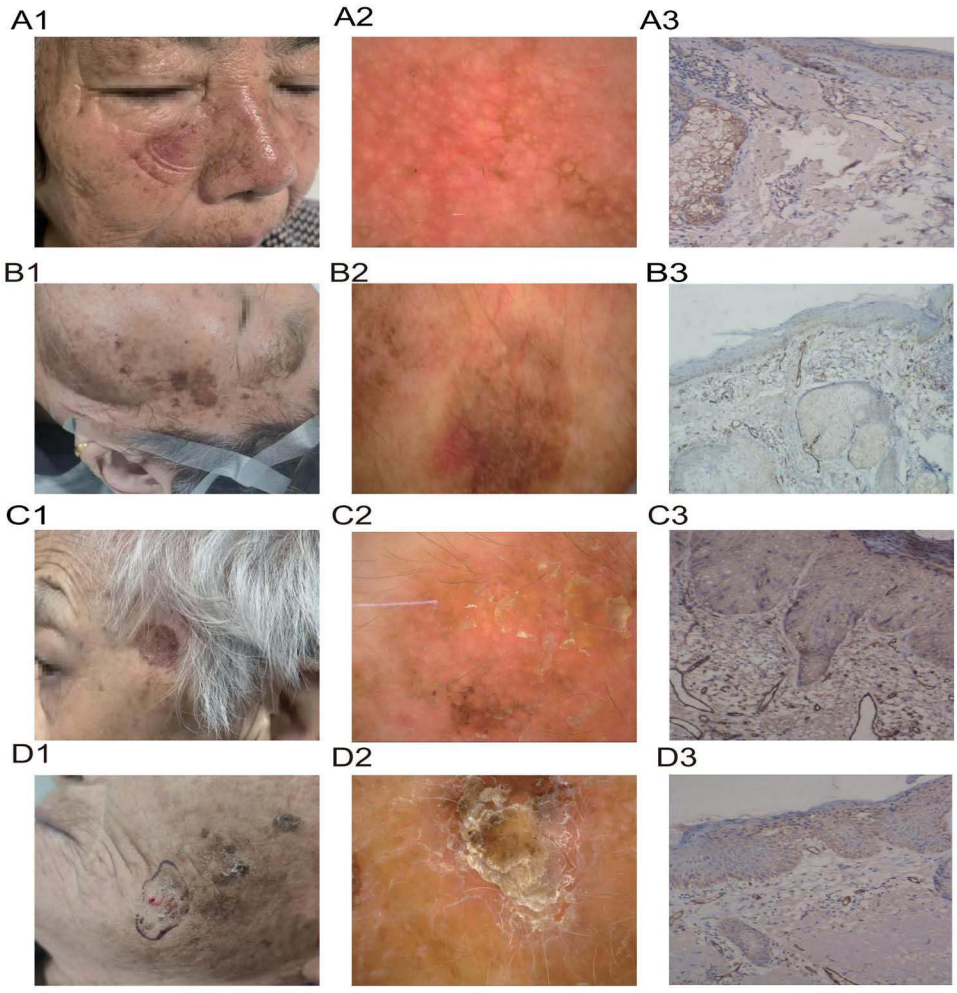

Figure 6 Representative images of AK cases. (**A1**–**D1**) These images clearly display the clinical manifestations of AK lesions. (**A2**–**D2**) Dermoscopic images of the corresponding lesions are presented here, highlighting characteristic dermoscopic features such as specific vascular patterns, perifollicular white halos, and scales. (**A3**–**D3**) These are the CD93 immunohistochemistry - stained histopathological images of AK tissues, visualizing the distribution and density of CD93 - positive microvessels within the lesions at the histological level (scale bar: 100μm).

https://doi.org/10.2147/OTT.S539790

Table 2 Relationship Between CD93-MVD and Clinical, Dermoscopic, and Pathological Characteristics of AK[a]

Characteristics	Groups	Number of Cases[n(%)]	CD93-MVD[b] (Vessels/HPF[c])	P-Value
Age(years)	≤65	22 (41.5)	19.00 (16.20,22.8)	0.042
	>65	31 (58.5)	24.00 (18.50,27.00)	
Gender	Fenmale	39 (73.6)	21.00 (17.00,25.50)	0.511
	Male	14 (26.4)	19.50 (17.00,23.50)	
number	Solitary	27(50.9)	19.00(17.00,22.50)	0.028
	Multiple	26(49.1)	24.00(19.00, 27.80)	
disease course (years)	≤1	13 (24.5)	19.0(17.00,24.00)	0.634
	>1	40 (75.5)	21.5(17.00,25.00)	
Clinical Classification	I	22 (41.5)	18.50(16.20,23.50)	0.040
	II	19 (35.9)	20.00 (17.00, 24.50)	
	III	12 (22.6)	24.00 (22.20, 31.20)	
Dermoscopic Classification	I	18 (34.0)	17.00 (16.00,21.80)	0.007
	II	25 (47.2)	20.00 (18.00, 25.00)	
	III	10 (18.9)	25.50 (23.20,31.80)	
Pathology Classification	I	25 (47.2)	21.80 (16.00,19.00)	2.3×10^{-6}
	II	18 (34.0)	25.00 (21.50,25.80)	
	III	10 (18.9)	31.8 (24.80,32.80)	

Notes: [a]AK: Actinic Keratosis. [b]CD93-MVD: CD93-positive Microvessel Density. [c]HPF: High Power Field.

dendritic cells, macrophages, eosinophils, mast cells, and neutrophils were observed in AK patients. By contrast, activated monocytes exhibited higher infiltration rates in controls (Figure 8A and B). ssGSEA analysis of neutrophil-related pathways (neutrophil signaling, neutrophil degranulation, and neutrophil granule composition) revealed significantly enhanced pathway activity in AK versus controls (Figure 8C and D). Correlation analysis further showed a significant positive association between CD93 expression and both neutrophil degranulation and granule composition pathways (Figure 8E).

Drug–Protein Interaction and Molecular Docking Analysis of NETs-Related Biomarkers

Targeting CD93 for therapeutic drug development represents an innovative approach for treating AK. Based on the STITCH database, a compound, C24H20N4O, was identified as a potential CD93-targeting drug (Figure 9A). Subsequently, docking studies were conducted to evaluate the binding potential of C24H20N4O (PubChem CID:3501) to the CD93 protein (PDB ID:8A59), with the 3D and 2D docking models shown in Figure 9B.

Discussion

NETs have been shown to be centrally implicated in the pathophysiological mechanisms of numerous clinical conditions, spanning autoimmune pathologies and neoplastic malignancies, as evidenced by accumulating scientific investigations.[8,35] In AK, given the established roles of inflammatory cascades and immune dysregulation, investigating NETs and their related biomarkers is highly necessary. Such investigations could elucidate underlying disease mechanisms, assess the progression, and develop targeted treatment strategies.

In this study, we obtained the datasets related to AK from the GEO database. We screened out DEGs and intersected them with NRGs to identify DE-NETs. Subsequently, functional enrichment analyses were conducted to systematically

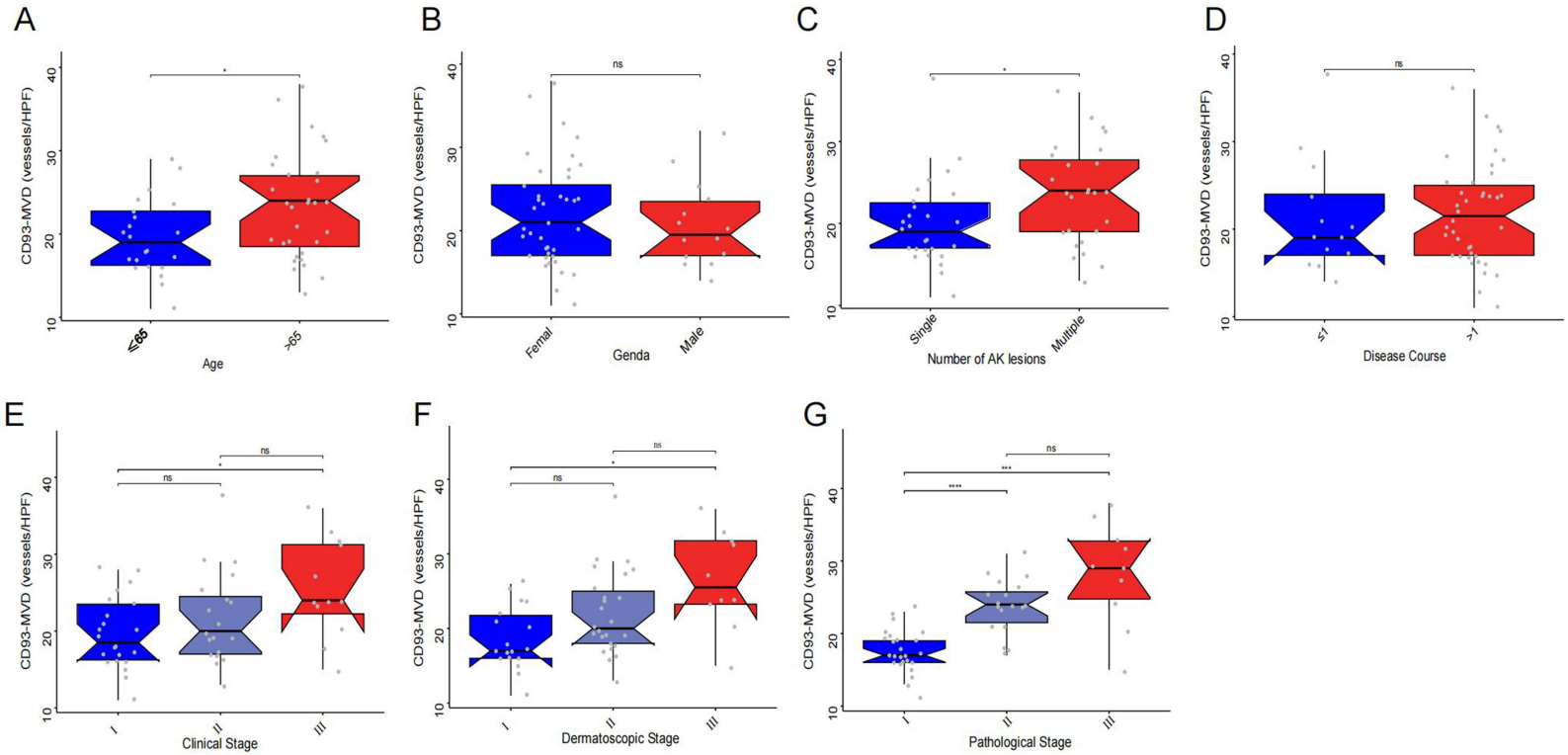

Figure 7 Box plots present the relationships between CD93 - MVD and different characteristics. (**A**–**D**) Respectively, these box plots compare CD93 - MVD in different age groups (≤65 years old vs >65 years old), between genders, according to disease course (≤1 year vs >1 year), and according to the number of lesions (solitary vs multifocal lesions). (**E**–**G**) These box plots illustrate the progressive elevation of CD93 - MVD with ascending severity grades in clinical, dermoscopic, and pathological classification systems. *p<0.05; **p<0.01; ***p<0.001; ****p<0.0001.

https://doi.org/10.2147/OTT.S539790

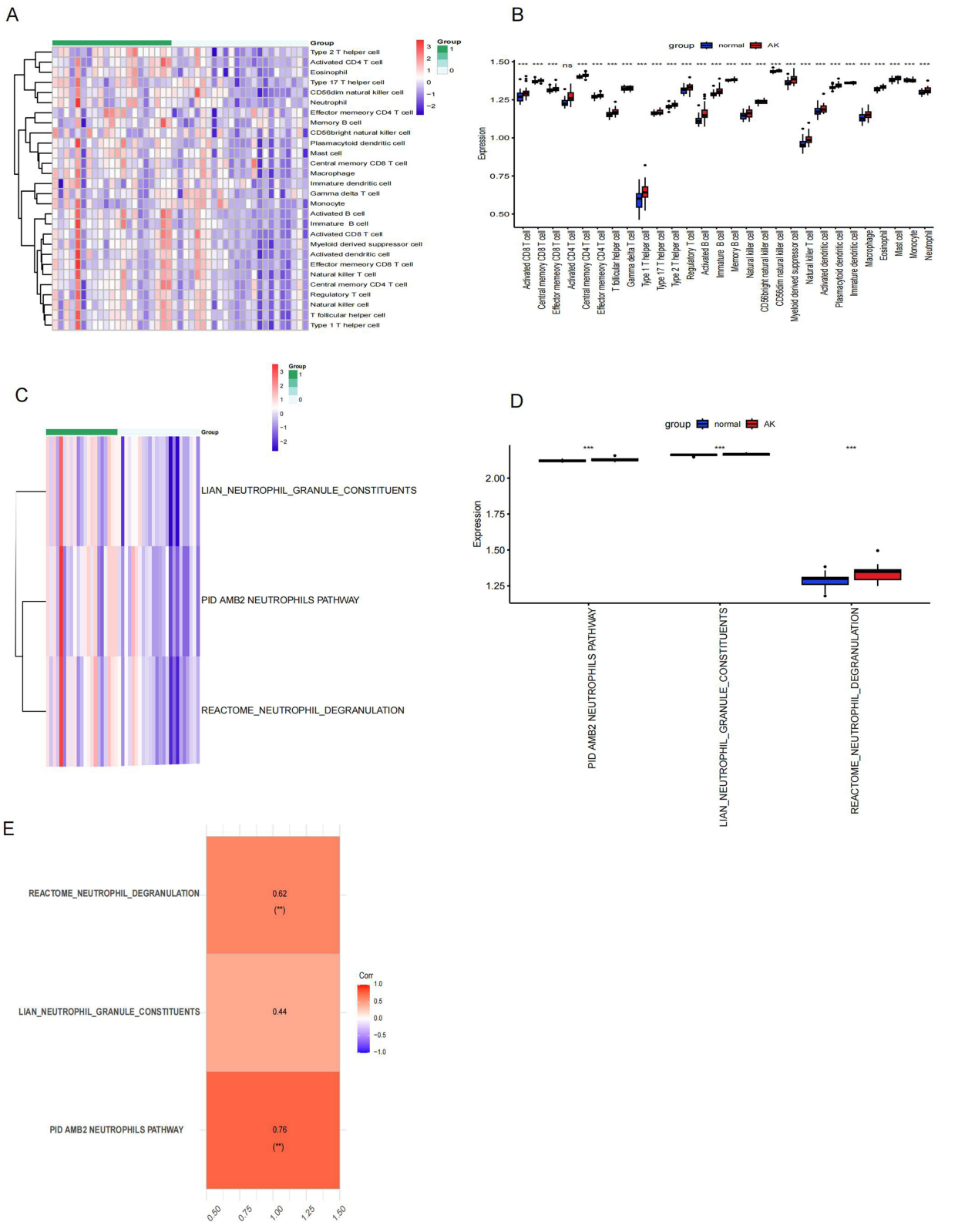

Figure 8 The ssGSEA method was employed to analyze changes in immune infiltration and neutrophil-related pathways. (**A**) Heat map illustrating differences in the distribution of 28 immune cell types across samples. (**B**) Box plots showing the differences in immune cell distributions between the control and AK groups. (**C**) Heat map depicting differences in the distribution of three neutrophil-related pathways across samples. (**D**) Box plot comparing ssGSEA scores of neutrophil-related pathways between the control and AK groups. (**E**) Correlation analysis of CD93 with the three neutrophil-related pathways.*p<0.05; **p<0.01; ***p<0.001; ****p<0.0001.

 https://doi.org/10.2147/OTT.S539790

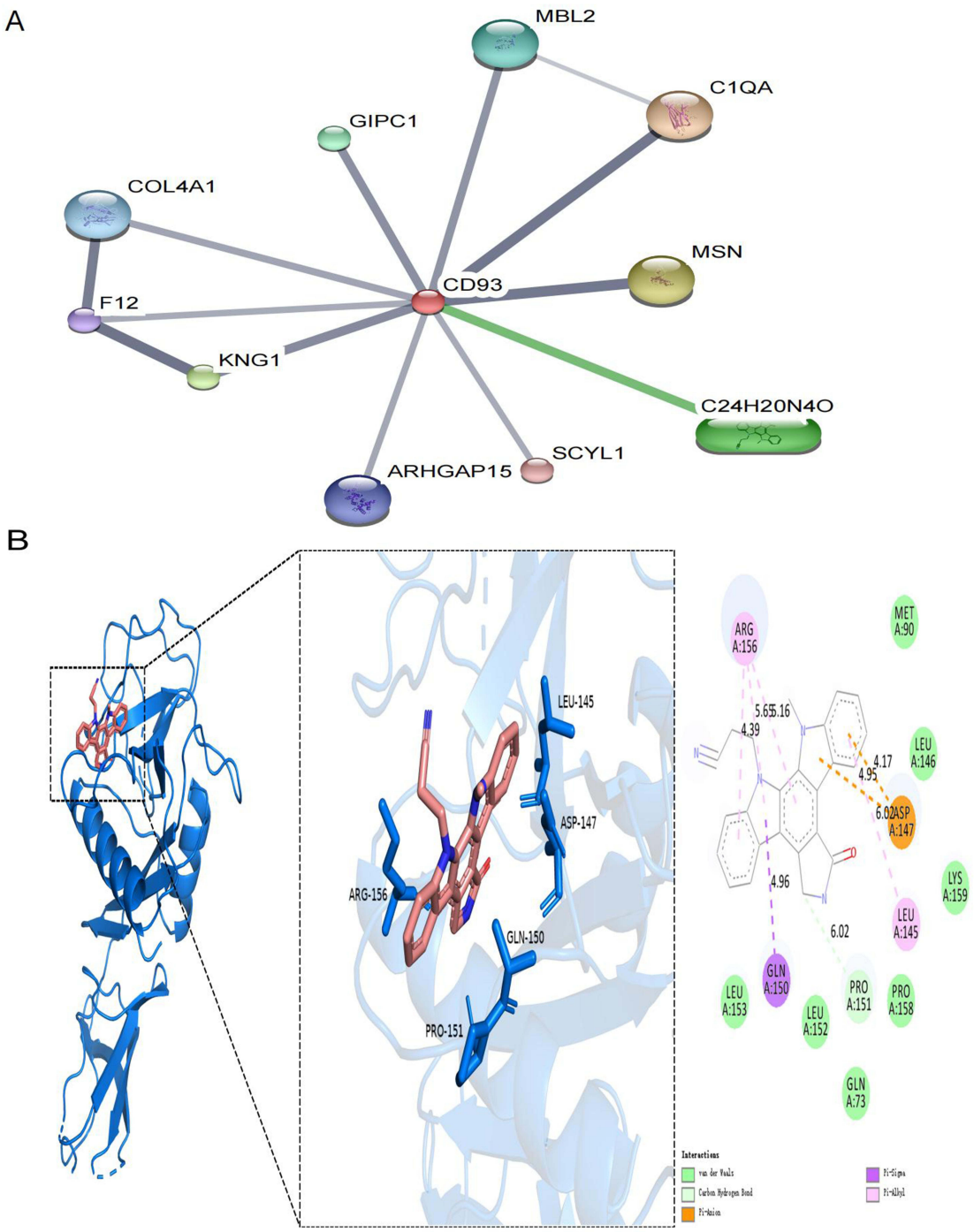

Figure 9 Interaction network and molecular docking analysis of CD93 with related proteins and compounds. (**A**) Interaction between CD93 and compound C24H20N4O (Gö6976). (**B**) Molecular docking model of CD93 with compound C24H20N4O (Gö6976), including an overall view of the docking, a close-up view of the docking and a 2D interaction diagram.

characterize the biological functions of these genes alongside the signaling pathways they engage in. We found that DE-NETs mainly focus on aspects such as neutrophil chemotaxis, migration, IL-17-mediated signaling, and PI3K-Akt pathway regulation. After clarifying the potential mechanism of DE-NETs in AK, we used machine learning algorithms to screen out CD93 as a key diagnostic biomarker for AK.

Encoded by the 20p11.21-located gene, CD93 is a transmembrane glycoprotein composed of 652 amino acids, existing as soluble and membrane-associated forms with primary expression in endothelial cell populations.

https://doi.org/10.2147/OTT.S539790

Angiogenesis promotion in physiological and disease states is mediated by this molecule, which is additionally linked to adverse prognosis, immunotherapy efficacy, immune cell trafficking, and high-grade TNM classification in cancer patients.[36] Studies demonstrate that CD93 binds to β-dystroglycan to activate Src kinase, thereby promoting endothelial cell migration and capillary-like structure formation via the Cbl/Rho/Rac signaling pathway.[37] Additionally, CD93 interacts with vascular endothelial cadherin (VE-cadherin) to maintain vascular barrier stability, and its loss results in increased vascular permeability.[38] The EGF-like domain of soluble cluster of sCD93 drives the proliferation of endothelial cells via the focal adhesion kinase (FAK)/phosphoinositide 3-kinase (PI3K)/protein kinase B (Akt)/endothelial nitric oxide synthase (eNOS)/extracellular signal-regulated kinase 1 and 2 (ERK1/2) signaling cascade, thereby orchestrating matrix metalloproteinase 2 (MMP2) upregulation to promote extracellular matrix degradation.[39] Immunohistochemical analysis revealed that CD93-MVD was significantly elevated in AK lesions when compared to normal cutaneous tissues ($P<0.05$). Elevated CD93-MVD was observed in AK patients with advanced age, multiple lesions, and higher clinical, dermoscopic, and pathological grades, suggesting that CD93-mediated pro-angiogenic activity may drive disease progression in AK.

AK is a well-established precancerous lesion of cSCC, yet the mechanisms underlying its malignant transformation to cSCC remain incompletely elucidated. In the present study, gradient changes in CD93-MVD levels were observed in AK lesions, and this phenomenon provides an entry point for exploring its role in the process of AK malignant transformation. Mechanistically, CD93-mediated increased angiogenesis has been confirmed to be closely associated with malignant tumor phenotypes, which can lay the foundation for tumor growth and metastasis by promoting neovascularization.[36] Although direct evidence linking CD93-MVD levels to cSCC progression remains limited, the correlation of CD93 with aggressive phenotypes in other malignancies provides theoretical support for its potential as a predictive marker for AK transformation to cSCC. Combined with the gradient changes in CD93-MVD levels observed across different AK grades in this study, this suggests that CD93 may be involved in the process of malignant transformation of AK to cSCC by regulating angiogenesis.Therefore, we will conduct targeted studies to verify this hypothesis, aiming to clarify the role and mechanism of CD93 in the malignant transformation of AK to cSCC.

Subsequently, immune cell infiltration and neutrophil-related signaling pathways were analyzed in two sample sets. In AK samples, elevated immune cell infiltration was observed, comprising activated CD8+ T cells (including central memory, effector memory subsets), CD4+ T cell populations (central memory, effector memory, follicular helper, Th1, Th17 subsets), γδ T cells, and neutrophils. Concurrently, neutrophil-related pathway activity was significantly upregulated in AK specimens. Of particular significance, CD93 expression exhibited a marked positive correlation with both neutrophil degranulation and neutrophil granule constituent pathways. This intimate association implies that CD93 may exert a pivotal role in AK pathogenesis by modulating neutrophil functions. Neutrophils with abnormal degranulation and granule composition pathways are likely to induce dysregulation of inflammatory responses and tissue damage. The positive correlation between CD93 and neutrophil pathways offers a novel clue to NETs' role in AK. Since NETs release is closely associated with neutrophil function, CD93-mediated modulation of these pathways may influence NET biogenesis, thus highlighting potential therapeutic targets for AK.

In light of this, we further predicted the CD93-directed therapeutics to facilitate the development of novel AK treatment strategies. Through the interaction and molecular docking analysis of CD93 protein with molecules and compounds, we found that the compound C24H20N4O (namely Gö6976) may be a potential targeted drug. Gö6976, a representative indolocarbazole agent, is commonly used as a selective PKCα/β inhibitor and demonstrates robust antitumor effects.[40,41] In chronic myeloid leukemia (CML) treatment, it has demonstrated promising therapeutic effects.[42] Additionally, preclinical evidence suggests its potential in managing dilated cardiomyopathy (DCM).[43] Currently, the therapeutic approaches for AK primarily include cryotherapy, laser therapy, surgical resection, photodynamic therapy, and topical agents such as imiquimod.[44] For multiple AKs, the discovery of targeted drugs undoubtedly provides new possibilities for better treatment options.However, the therapeutic effect of Gö6976 on AK still requires more in-depth research for confirmation, with the hope of bringing the greatest benefit to AK treatment.

Although this study has achieved a series of meaningful results, it should be acknowledged that certain limitations remain. Our study predominantly relies on bioinformatics analysis, and experimental validation via in vitro and in vivo models is currently lacking. In subsequent studies, we will carry out more experimental validations to explore the

mechanisms by which CD93 and NETs interact and contribute to AK pathogenesis, thus providing stronger evidence for AK diagnosis and treatment.

Conclusion

In short, this study successfully identified CD93 as a potential NETs-related diagnostic marker for AK and highlighted its key role in immune infiltration and neutrophil-related pathways. CD93 has been identified via molecular docking as a potential therapeutic target for AK, which may foster the development of targeted treatment strategies.

Abbreviations

AK, Actinic Keratosis; cSCC, Cutaneous Squamous Cell Carcinoma; NETs, Neutrophil Extracellular Traps; DEGs, Differentially Expressed Genes; NRGs, NETs-Related Genes; GO,Gene Ontology; KEGG, Kyoto Encyclopedia of Genes and Genomes; ssGSEA, Single-sample Gene Set Enrichment Analysis; LASSO, Least Absolute Shrinkage and Selection Operator; RF, Random Forest; SVM-RFE, Support Vector Machine Recursive Feature Elimination; ROC, Receiver Operating Characteristic Curve; AUC, Area Under the Curve; CD93-MVD, CD93-positive Microvessel Density.

Data Sharing Statement

The data used in this study is freely available in the GEO online database (https://www.ncbi.nlm.nih.gov/geo/). Our analyses, protocols, raw figures, or other information related to this study could be requested from the corresponding author(s) upon reasonable request.

Ethics Statement

This study was approved by the Ethics Committee of the First Affiliated Hospital of Wannan Medical College (No. 2024-178).All human participants provided signed informed consent, including written authorization for the publication of study details. The research complied with the ethical principles of the Declaration of Helsinki. In particular, the patients in Figure 6 have provided written informed consent for the publication of their images.

Acknowledgments

We extend our gratitude to colleagues not listed as authors for their contributions to this study. We also acknowledge the support provided by the institutions and departments involved.

Author Contributions

All authors made a significant contribution to the work reported, whether that is in the conception, study design, execution, acquisition of data, analysis and interpretation, or in all these areas; took part in drafting, revising or critically reviewing the article; gave final approval of the version to be published; have agreed on the journal to which the article has been submitted; and agree to be accountable for all aspects of the work.

Funding

This study was funded by the following projects: The Natural Science Foundation of Universities in Anhui Province (2023AH051781); The Key Research Projects Fund of Wannan Medical College (WK2024ZZD30).

Disclosure

The authors report no conflicts of interest in this work.

References

1. Lee YB, Kim JI. Genetic Studies of Actinic Keratosis Development: where Are We Now? *Ann Dermatol*. 2023;35(6):389–399. doi:10.5021/ad.23.072
2. Criscione VD, Weinstock MA, Naylor MF, Luque C, Eide MJ, Bingham SF. Actinic keratoses: natural history and risk of malignant transformation in the Veterans Affairs Topical Tretinoin Chemoprevention Trial. *Cancer*. 2009;115(11):2523–2530. doi:10.1002/cncr.24284

3. Reinehr CPH, Bakos RM. Actinic keratoses: review of clinical, dermoscopic, and therapeutic aspects. *An Bras Dermatol*. 2019;94(6):637–657. doi:10.1016/j.abd.2019.10.004
4. Scapini P, Cassatella MA. Social networking of human neutrophils within the immune system. *Blood*. 2014;124(5):710–719. doi:10.1182/blood-2014-03-453217
5. Warino L, Tusa M, Camacho F, Teuschler H, Fleischer Jr AB, S.r F. Frequency and cost of actinic keratosis treatment. *Dermatol Surg*. 2006;32 (8):1045–1049. doi:10.1111/j.1524-4725.2006.32228.x
6. Masucci MT, Minopoli M, Del Vecchio S, Carriero MV. The Emerging Role of Neutrophil Extracellular Traps (NETs) in Tumor Progression and Metastasis. *Front Immunol*. 2020;11:1749. doi:10.3389/fimmu.2020.01749
7. Papayannopoulos V. Neutrophil extracellular traps in immunity and disease. *Nat Rev Immunol*. 2018;18(2):134–147. doi:10.1038/nri.2017.105
8. Mutua V, Gershwin LJ. A Review of Neutrophil Extracellular Traps (NETs) in Disease: potential Anti-NETs Therapeutics. *Clin Rev Allergy Immunol*. 2021;61(2):194–211. doi:10.1007/s12016-020-08804-7
9. Hirota T, Levy JH, Iba T. The influence of hyperglycemia on neutrophil extracellular trap formation and endothelial glycocalyx damage in a mouse model of type 2 diabetes. *Microcirculation*. 2020;27(5):e12617. doi:10.1111/micc.12617
10. Glennon-Alty L, Hackett AP, Chapman EA, Wright HL. Neutrophils and redox stress in the pathogenesis of autoimmune disease. *Free Radic Biol Med*. 2018;125:25–35. doi:10.1016/j.freeradbiomed.2018.03.049
11. Odqvist L, Jevnikar Z, Riise R, et al. Genetic variations in A20 DUB domain provide a genetic link to citrullination and neutrophil extracellular traps in systemic lupus erythematosus. *Ann Rheum Dis*. 2019;78(10):1363–1370. doi:10.1136/annrheumdis-2019-215434
12. Mitroulis I, Kambas K, Chrysanthopoulou A, et al. Neutrophil extracellular trap formation is associated with IL-1β and autophagy-related signaling in gout. *PLoS One*. 2011;6(12):e29318. doi:10.1371/journal.pone.0029318
13. Modestino L, Cristinziano L, Trocchia M, et al. Melanoma-derived soluble mediators modulate neutrophil biological properties and the release of neutrophil extracellular traps. *Cancer Immunol Immunother*. 2023;72(10):3363–3376. doi:10.1007/s00262-023-03493-5
14. Moeller LH, Weishaupt C, Schedel F. Evidence of Neutrophils and Neutrophil Extracellular Traps in Human NMSC with Regard to Clinical Risk Factors, Ulceration and CD8+ T Cell Infiltrate. *Int J Mol Sci*. 2024;25(19):10620. doi:10.3390/ijms251910620
15. Zhang Y, Guo L, Dai Q, et al. A signature for pan-cancer prognosis based on neutrophil extracellular traps. *J Immunother Cancer*. 2022;10(6): e004210. doi:10.1136/jitc-2021-004210
16. Dubois-Pot-Schneider H, Khairallah G, Brzenczek C, Plénat F, Marchal F, Amouroux M. Transcriptomic Study on Human Skin Samples: identification of Two Subclasses of Actinic Keratoses. *Int J Mol Sci*. 2023;24(6):5937. doi:10.3390/ijms24065937
17. Segura S, Gadea A, Nonell L, et al. Identification of differentially expressed genes in actinic keratosis samples treated with ingenol mebutate gel. *PLoS One*. 2020;15(5):e0232146. doi:10.1371/journal.pone.0232146
18. Hameetman L, Commandeur S, Bavinck JN, et al. Molecular profiling of cutaneous squamous cell carcinomas and actinic keratoses from organ transplant recipients. *BMC Cancer*. 2013;13(1):58. doi:10.1186/1471-2407-13-58
19. Joly F, Deret S, Gamboa B, et al. Photodynamic therapy corrects abnormal cancer-associated gene expression observed in actinic keratosis lesions and induces a remodeling effect in photodamaged skin. *J Dermatol Sci*. 2018;91(2):206–218. doi:10.1016/j.jdermsci.2018.05.002
20. Anders S, Huber W. Differential expression analysis for sequence count data. *Genome Biol*. 2010;11(10):R106. doi:10.1186/gb-2010-11-10-r106
21. Gene Ontology Consortium. Gene Ontology Consortium: going forward. *Nucleic Acids Res*. 2015;43(Database issue):D1049–D1056. doi:10.1093/nar/gku1179
22. Kanehisa M, Furumichi M, Sato Y, Kawashima M, Ishiguro-Watanabe M. KEGG for taxonomy-based analysis of pathways and genomes. *Nucleic Acids Res*. 2023;51(D1):D587–D592. doi:10.1093/nar/gkac963
23. Wu T, Hu E, Xu S, et al. clusterProfiler 4.0: a universal enrichment tool for interpreting omics data. *Innovation*. 2021;2(3):100141. doi:10.1016/j.xinn.2021.100141
24. Cao X, He J, Chen A, et al. Comprehensive analysis of necroptosis landscape in skin cutaneous melanoma for appealing its implications in prognosis estimation and microenvironment status. *J Pers Med*. 2023;13(2):245. doi:10.3390/jpm13020245
25. Wei C, Wei Y, Cheng J, et al. Identification and verification of diagnostic biomarkers in recurrent pregnancy loss via machine learning algorithm and WGCNA. *Front Immunol*. 2023;14:1241816. doi:10.3389/fimmu.2023.1241816
26. Sundermann B, Bode J, Lueken U, et al. Support Vector Machine Analysis of Functional Magnetic Resonance Imaging of Interoception Does Not Reliably Predict Individual Outcomes of Cognitive Behavioral Therapy in Panic Disorder with Agoraphobia. *Front Psychiatry*. 2017;8:99. doi:10.3389/fpsyt.2017.00099
27. Robin X, Turck N, Hainard A, et al. pROC: an open-source package for R and S+ to analyze and compare ROC curves. *BMC Bioinform*. 2011;12 (1):77. doi:10.1186/1471-2105-12-77
28. Shen Y, Wu Y, Hao M, et al. Clinicopathological association of CD93 expression in gastric adenocarcinoma. *J Cancer Res Clin Oncol*. 2024;150 (8):400. doi:10.1007/s00432-024-05874-4
29. Weidner N, Folkman J, Pozza F, et al. Tumor angiogenesis: a new significant and independent prognostic indicator in early-stage breast carcinoma. *J Natl Cancer Inst*. 1992;84(24):1875–1887. doi:10.1093/jnci/84.24.1875
30. Chen Y, Feng Y, Yan F, Zhao Y, Zhao H, Guo Y. A Novel Immune-Related Gene Signature to Identify the Tumor Microenvironment and Prognose Disease Among Patients With Oral Squamous Cell Carcinoma Patients Using ssGSEA: a Bioinformatics and Biological Validation Study. *Front Immunol*. 2022;13:922195. doi:10.3389/fimmu.2022.922195
31. Ezaouine A, Salam MR, Nouadi B, et al. In Silico Prediction of the Bioactive Profile and Metabolites of Satureja nepeta in Diseases Related to the Excessive Production of Interleukin-6. *Bioinform Biol Insights*. 2022;16:11779322221115665. doi:10.1177/11779322221115665
32. Liu T, Zhuang XX, Gao JR. Identifying Aging-Related Biomarkers and Immune Infiltration Features in Diabetic Nephropathy Using Integrative Bioinformatics Approaches and Machine-Learning Strategies. *Biomedicines*. 2023;11(9):2454. doi:10.3390/biomedicines11092454
33. Wang Y, Bryant SH, Cheng T, et al. PubChem BioAssay: 2017 update. *Nucleic Acids Res*. 2017;45(D1):D955–D963. doi:10.1093/nar/gkw1118
34. Nguyen NT, Nguyen TH, Pham TNH, et al. Autodock Vina Adopts More Accurate Binding Poses but Autodock4 Forms Better Binding Affinity. *J Chem Inf Model*. 2020;60(1):204–211. doi:10.1021/acs.jcim.9b00778
35. Guan X, Zhao Z, Yan H, Yan H. NETs: important players in cancer progression and therapeutic resistance. *Exp Cell Res*. 2024;441(2):114191. doi:10.1016/j.yexcr.2024.114191
36. Tossetta G, Piani F, Borghi C, Marzioni D. Role of CD93 in Health and Disease. *Cells*. 2023;12(13):1778. doi:10.3390/cells12131778

37. Galvagni F, Nardi F, Maida M, et al. CD93 and dystroglycan cooperation in human endothelial cell adhesion and migration adhesion and migration. *Oncotarget*. 2016;7(9):10090–10103. doi:10.18632/oncotarget.7136
38. Lugano R, Vemuri K, Barbera S, et al. CD93 maintains endothelial barrier function by limiting the phosphorylation and turnover of VE-cadherin. *FASEB J*. 2023;37(4):e22894. doi:10.1096/fj.202201623RR
39. Kao YC, Jiang SJ, Pan WA, et al. The epidermal growth factor-like domain of CD93 is a potent angiogenic factor. *PLoS One*. 2012;7(12):e51647. doi:10.1371/journal.pone.0051647
40. Merzoug-Larabi M, Spasojevic C, Eymard M, et al. Protein kinase C inhibitor Gö6976 but not Gö6983 induces the reversion of E- to N-cadherin switch and metastatic phenotype in melanoma: identification of the role of protein kinase D1. *BMC Cancer*. 2017;17(1):12. doi:10.1186/s12885-016-3007-5
41. Yao J, Zhao X, Ding X. Systematic profiling of chemotherapeutic drug response to EGFR gatekeeper mutation in non-small cell lung cancer. *Comput Biol Chem*. 2016;64:126–133. doi:10.1016/j.compbiolchem.2016.05.009
42. Cao ZR, Chen XP, Feng M, et al. The effect of Gö6976 on chronic myeloid leukemia in vitro and in vivo. *Hematology*. 2021;26(1):543–551. doi:10.1080/16078454.2021.1945235
43. Perea-Gil I, Seeger T, Bruyneel AAN, et al. Serine biosynthesis as a novel therapeutic target for dilated cardiomyopathy. *Eur Heart J*. 2022;43(36):3477–3489. doi:10.1093/eurheartj/ehac305
44. Dianzani C, Conforti C, Giuffrida R, et al. Current therapies for actinic keratosis. *Int J Dermatol*. 2020;59(6):677–684. doi:10.1111/ijd.14767